Research Article Vol. 30, No. 3 / 31 Jan 2022 / Optics Express 3404

Optics EXPRESS

Spatio-spectral couplings in saturated collinear OPCPA

TIMO EICHNER,[1,*] THOMAS HÜLSENBUSCH,[1,2] JULIAN DIRKWINKEL,[2] TINO LANG,[2] LUTZ WINKELMANN,[2] GUIDO PALMER,[2] AND ANDREAS R. MAIER[2]

[1] *Center for Free-Electron Laser Science and Department of Physics, University of Hamburg, Luruper Chaussee 149, 22761 Hamburg, Germany*
[2] *Deutsches Elektronen-Synchrotron DESY, Notkestr. 85, 22607 Hamburg, Germany*
[*] *timo.eichner@cfel.de*

Abstract: Ultrafast laser pulses featuring both high spatio-temporal beam quality and excellent energy stability are crucial for many applications. Here, we present a seed laser with high beam quality and energy stability, based on a collinear optical parametric chirped pulse amplification (OPCPA) stage, delivering 46 μJ pulses with a 25 fs Fourier limit at 1 kHz repetition rate. While saturation of the OPCPA stage is necessary for achieving the highest possible energy stability, it also leads to a degradation of the beam quality. Using simulations, we show that spectrally dependent, rotationally symmetric aberrations dominate the collinear OPCPA in saturation. We experimentally characterize these aberrations and then remove distinct spatial frequencies to greatly improve the spectral homogeneity of the beam quality, while keeping an excellent energy stability of 0.2 % rms measured over 70 hours.

1. Introduction

The combination of high spatio-temporal beam quality and high energy stability are essential for a variety of high-intensity laser applications ranging from ultrafast spectroscopy [1,2] and microscopy [3] to laser-plasma acceleration (LPA) [4,5]. In general, spatio-temporal coupling (STC) reduce the peak intensity of the laser at the interaction point and, therefore, should be kept to a minimum. In the case of LPA, spatio-temporal couplings such as pulse front tilt (PFT), and angular or spatial chirp, can lead to an asymmetry of the plasma dynamics which can steer a plasma-accelerated electron beam [6–9]. Furthermore, the bulk of shot-to-shot variations in the LPA electron beam can be linked to fluctuations of the drive pulse properties [10,11].

Dispersive optical elements, such as compressor gratings, have been studied as sources of STCs [12,13]. However, spatio-temporal couplings can already be introduced in early stages of a high-energy laser system. The requirement of high stability in combination with high beam quality therefore poses strict demands on the whole amplifier system, starting with the seed laser system.

Optical parametric chirped pulse amplification (OPCPA) [14] is often used as an alternative to more conventional Ti:Sapphire based regenerative amplifiers that are commonly found in the low energy front-end of high intensity laser systems [15–17]. Compared to Ti:Sapphire technology, OPCPA has many advantages such as compactness, due to the high gain achievable over short propagation lengths, and the possibility to tune the spectral properties of the output pulses [16]. In addition, OPCPA based laser systems have an inherently high temporal contrast and do not suffer from gain narrowing or some of the thermal issues that limit the high power operation of some laser systems [18,19].

For applications that demand sub-10 fs pulses, non-collinear optical parametric amplification (NOPA) additionally offers an extraordinarily high gain bandwidth [20–22]. The output of NOPA systems however has an inherent pulse front tilt and spatial chirp [23], which has some

#448551 https://doi.org/10.1364/OE.448551
Journal © 2022 Received 15 Nov 2021; revised 7 Jan 2022; accepted 11 Jan 2022; published 18 Jan 2022

disadvantages for driving LPAs. These STCs can, in principle, be prevented by matching the pulse front of the pump and the seed [24], or by fine-tuning the size of pump and seed [23] and the non-collinear angles [25].

Instead, collinear OPA (COPA) maintains an axial symmetry of the interacting pulses which eliminates the inherent tendency for an angular or spatial chirp. Thereby, higher pulse quality can be achieved without the complexity of additional preventive measures required by NOPAs. The trade-off is in the phase matching bandwidth, which is significantly lower in the collinear case, but still sufficient to provide pulse durations in the 15-20 fs range which is enough for seeding many high-energy Ti:Sapphire systems. Yet, for many applications that simply require peak intensity, the benefit of the shorter pulse duration supported by a NOPA scheme, outweighs the slight degradation of the peak intensity that is expected from spatio-temporal distortion of the pulses, making NOPA-based seeders a popular choice for many applications.

For LPAs, however, the pulse quality in combination with stability of the pulse properties is an essential figure of merit [10,11]. Due to the highly nonlinear laser-plasma interaction, the laser-plasma acceleration process is extremely sensitive to the input pulse properties. Therefore, with OPCPA-based seeders, highly stable pump lasers and a strong saturation of the parametric amplification process [19,26] is required. The drawback of saturation, however, is a degradation of the pulses spatial profile and its phase properties. The coupling of both effects has to be carefully studied [27].

The spatio-temporal Strehl-ratio of a saturated NOPA has been studied in [28] and the introduction of STCs through parametric phase has recently been investigated in [29]. However, to the best of our knowledge, spectrally resolved measurements of a COPA operated in saturation have not yet been presented.

Here, we will present a collinear OPCPA system that has been designed for high stability operation. Using simulations, we study the deformation of the amplified pulse and then present measurements which verify the presence of spectrally dependent aberrations in the pulse. Finally, we show that spatial filtering can greatly improve the uniformity of the beam quality across the spectrum of the amplified pulses.

2. Experimental setup and laser performance

The OPCPA based laser system was designed to seed a 100 TW-class Ti:Sapphire laser system, similar to systems that are being used in laser-plasma acceleration [30]. The design focuses on providing high stability in combination with high beam quality. Other features such as conversion efficiency did not play a role.

The general layout of the collinear OPCPA system is shown in Fig. 1. It is driven by an industrial Yb-doped laser (Pharos-SP, Light Conversion) delivering a positively chirped 500 fs pulse with 1 mJ of pulse energy at a 1 kHz repetition rate. The pump laser was primarily chosen for its high pulse-to-pulse energy stability, measured to be about 0.3 % rms. The pump laser also has a high beam quality with a Gaussian profile and an M^2 of 1.07 and 1.12 in the vertical and horizontal axes.

The majority of the pulse is sent into a β-barium borate (BBO) crystal for second harmonic generation (SHG). The SHG conversion efficiency amounts to 44 % and is strongly limited by the chirp of the pulse, as well as the constraint of maintaining a low input intensity to prevent long term damage of the crystal. Before the SHG, 1 μJ of the pulse is split off, compressed to the Fourier limit of approximately 170 fs, and focused into a bulk YAG crystal for white light generation (WLG) [31]. The white light with a pulse energy of around 2.5 nJ in the 750-850 nm spectral range is then amplified in two subsequent OPA stages (OPA1 and OPA2) that are pumped by the SHG output. As a non-linear material, lithium triborate (LBO) was chosen in type 1 critical phase matching, since it provides a slightly larger phase-matching bandwidth and a smaller birefringent walk-off angle than comparable materials such as BBO.

Optics EXPRESS

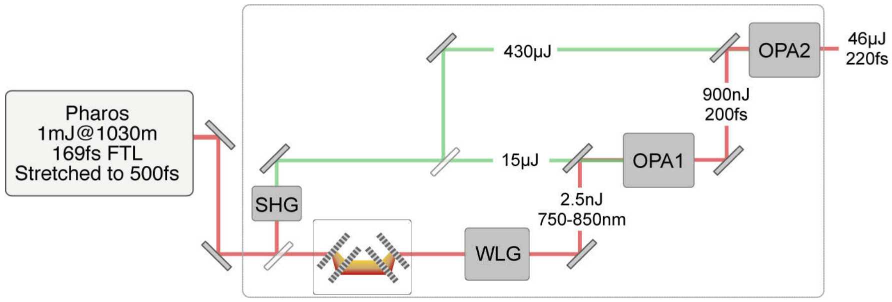

Fig. 1. Layout the of the collinear OPCPA seed laser. It is pumped by an industrial Yb-doped laser and consists of a two OPA staged seeded by white light generated in a bulk YAG crystal. See main text for further details.

The exact operation parameters of the amplification stages and the SHG were carefully adjusted with numerical start-to-end simulations using a (3+1)D non-linear pulse propagation model (chi3D). The chi3D simulation code is an extended version of the (2+1)D model presented in [32].

To achieve an optimum balance between output stability [26,33] and beam quality, a stable SHG and saturation of the second OPA stage are necessary, both of which were achieved through careful adjustment of crystal lengths and beam intensities. Furthermore, the gain of the two amplification stages is kept low (approx. 500 in OPA1 and 50 in OPA2) to prevent the degradation of stability and temporal contrast due to amplified parametric superfluorescence [18,34,35]. Additionally, superfluorescence was limited by adjusting the ratio of pump and seed pulse durations. This however entails a trade-off with the amplified bandwidth and can only be done to a limited degree [36].

The output of the first OPA stage has a Fourier limit of 20.5 fs and a pulse energy of 900 nJ. The spectrally integrated Strehl ratio is 0.94 and the M^2 was measured to be 1.05 in the horizontal and 1.03 in the vertical axes, indicating that there are no significant aberrations in the beam. This allows to isolate and illustrate the effect of saturation of the second OPA stage that is characterized in the following sections.

The output performance of the second amplifier of the laser system is shown in Fig. 2. It provides a pulse energy of 46 μJ with a rms shot-to-shot energy stability of 0.22% over 70 hours, including a one hour warm-up phase in the beginning. The short term pulse-to-pulse energy stability (calculated over one second) remains at a mean of 0.15% for the entire time of the 70 h measurement, making it very stable compared to similar systems [37–39]. The energy stability was measured with a photo-diode based sensor (Ophir PD10-C). Despite careful adjustment of the signal level and maximising the dynamic range of the sensor, the inherent noise of the measurement is at around 0.1%rms and therefore has a significant contribution to the determined stability.

The output spectrum of the OPCPA is centered at 800 nm with a 60 nm FWHM bandwidth, corresponding to a 24.8 fs Fourier transform limit. After compression with a chirped mirror compressor and a pair of fused silica wedges, the pulse duration was measured to be 25 fs with an intensity autocorrelator (assuming a Gaussian pulse profile), and 26.5 fs with frequency resolved optical gating (FROG). Both results indicate that there is no detrimental degradation of the spectral phase as a consequence of the saturation and the pulse is well compressible. The temporal intensity contrast was measured to be $>10^{10}$ at >500 fs before the pulse, confirming the absence superfluorescence or strong phase modulations. The contrast was measured using a third-order autocorrelator and limited by the dynamic range of the device.

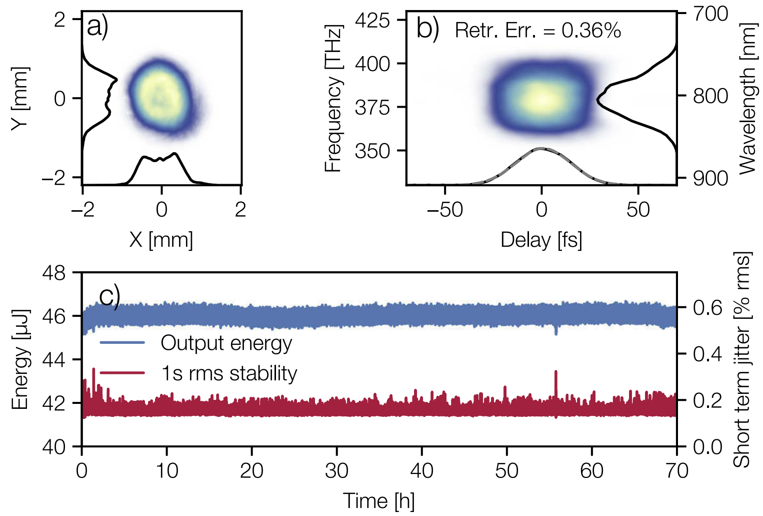

Fig. 2. Overview of laser parameters of the second OPA stage: a) beam profile at the output facet of the amplifier crystal, b) Measured raw FROG trace of the compressed pulse with the corresponding projections to the spectral and temporal axis. A Gaussian profile is fitted to the temporal axis (dashed grey line). c) Long term trends of the output pulse energy and short term energy jitter that has been calculated over one second. The measured stability of the OPCPA system is limited towards the low end by the inherent noise of the measurement system.

3. Simulation of beam quality in the saturation regime

In order to further understand the saturation dynamics in the second OPA stage, we modelled that stage using chi3D. As inputs to the simulation, spatially and temporally Gaussian pump and seed pulses were used, which well approximate the profiles measured in the laser. Besides that, the pulse properties and LBO crystal length (5.2 mm) were the same as the ones as in the laser system described in the previous section. The LBO was operated at a phase matching angle of $\Phi = 11.8°$ and $\Theta = 90°$.

Figure 3 illustrates the evolution of the pulse energy (and its variation δE for a 1 % pump energy fluctuation) in the second amplifier stage, as well as the spectral dependence of the beam profile and wavefront in the plane of birefringent walk-off at three snapshots along the propagation through the amplification crystal. Since there is no visible effect of the birgefringent walk-off between pump and seed in LBO crystal and the beam stays symmetric with respect to the beam axis, the pulse properties can for now be considered rotationally symmetric and the slices shown in the figure are indicative of the entire beam profile.

Figure 3 further shows, that the pulse energy stability improves only once the pulse energy starts to saturate. A crystal length where the tolerance towards pump fluctuations is optimal, is reached at 5.2 mm, i.e. at a value slightly beyond the working point with highest output energy [26]. The 5.2 mm crystal length was therefore chosen for OPA2.

As the pulse energy stability improves during the amplification, the beam profile strongly degrades and becomes dependent on the wavelength. At wavelengths near the center of the spectrum – which, due to its chirp, is equivalent to the temporal center of the pulse – the pump and seed intensities are highest, and the phase matching curve shows the highest relative conversion efficiency. Due to the combination of these factors, the central part of the spectrum reaches the back-conversion regime first. This back-conversion in the central high intensity part of the pulse then leads to (i) a change in the beam profile, and (ii) introduces a spatially varying parametric

Optics EXPRESS

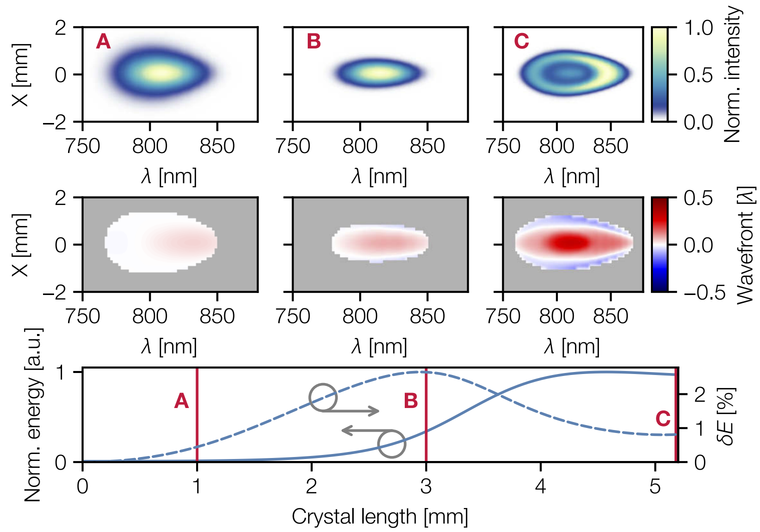

Fig. 3. Top row: snapshots of the spectrally dependent slices of the beam profile, middle: spectrally dependent slices of the wavefront error (limited to region with intensity larger than 10% of the peak intensity), bottom: the evolution of the seed energy (solid line) during propagation through the LBO crystal. To indicate the stability with respect to pump fluctuations, the relative variation in output energy (dashed line) is plotted on the right axis for a pump energy variation of 1%. A minimal variation of 0.8% (i.e. better than the pump stability) is reached at the exit of the crystal. The 5.2 mm crystal length, where the optimal pulse energy stability is reached, is also used as the working point for the OPCPA system. All results shown in this figure are simulated using chi3D.

phase [29,40]. In contrast, the edges of the pulse have less favorable conversion conditions, thus reach the back-conversion regime later during the amplification, and therefore maintain a higher beam quality until the end of the amplification.

Due to the coupling of the wavelength and temporal profile of the pulse, the parametric phase shift and change of beam profile lead to a wavelength dependent the wavefront and beam profile of the pulse, that is inherent to saturated OPCPA with pulses that have a temporally varying intensity (such as e.g. Gaussian pulses).

From a Zernike analysis of the wavefront of the amplified pulses, it is evident that the wavefront distortion introduced by the saturation primarily result in aberrations that have a rotational symmetry such as defocus and spherical aberrations. This can be seen in Fig. 4, where the Zernike coefficients of the fully saturated wavefront are shown. This rotational symmetry of the aberrations can be attributed to the collinear propagation of seed and pump pulses, and the resulting symmetry of the amplification process. The minor contribution of 4^{th} order coma that is visible in Fig. 4 is attributed to the slight breaking of the symmetry due to the small spatial walkoff. The analysis of the Zernike composition of the wavefront was done using the tools described in [12,41].

Optics EXPRESS

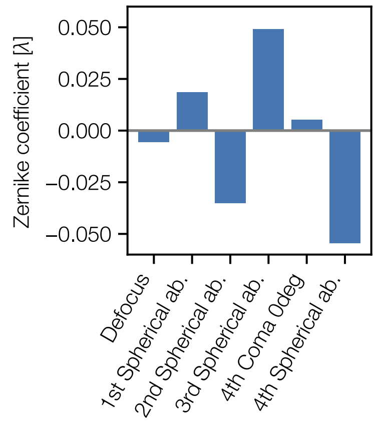

Fig. 4. Amplitude of the Zernike polynomials of the spectrally integrated wavefront. Only values with an amplitude larger than $\lambda/200$ and up to the 66th polynomial are shown. The amplified pulse primarily features rotationally symmetric aberrations.

4. Measurement of STCs and results

The aberrations expected from the simulations of the previous sections were experimentally characterized using the INSIGHT technique [42]. This method is based on two dimensional Fourier spectroscopy in combination with a phase retrieval approach to reconstruct the entire spatio-spectral electric field of the laser pulse. The method allows to identify complex spatio-spectral couplings in both the intensity and phase profiles of the pulse, and is therefore ideally suited to investigate the previously described aberrations [43].

For the INSIGHT measurements, the output surface of the OPA2 crystal was imaged with a 4f telescope consisting of two $f = 500$ mm achromatic lenses. A third achromatic lens with a focal length of 200 mm in the image plane was then used to focus the beam into the measurement device.

The near-field (NF) beam profiles that were reconstructed using the INSIGHT technique, are shown in the top of Fig. 5 and agree with the simulated beam profiles in the bottom row. The reconstructed NF beam profile also agrees with the directly measured NF beam profile shown in Fig. 2, indicating that the residual error of the reconstruction is low. This agreement is also quantified by a 6.7 % rms deviation between the retrieved and measured in-focus (far-field, FF) intensity profiles.

The same features in the FF and NF profiles are visible when comparing the measured and simulated beams. The beam profile strongly deviates from a Gaussian profile near the center of the spectrum, resulting in characteristic side-lobes in the far-field, while the edges of the spectrum maintain a high beam quality. In the amplifier crystal (i.e. close to the NF plane), the center of the pulse is depleted as a consequence of back-conversion, resulting in a dip in the beam profile. The spectrally integrated beam profile shows a flat top shape that is expected from the simulation. As expected from the collinear design of the OPA system, no spatial or angular dispersion is observed in the beam. In the wavefront, a strong phase shift is visible in the areas of the pulse, where back-conversion occurs, resulting in the expected radially symmetric wavefront aberrations. The discrepancy between the measured and simulated wavefronts is attributed to Kerr-lensing in the pump pulse that leads to a sharper intensity peak than the Gaussian assumed in the simulation. This sharper peak leads to a more localized distortion of the wavefront.

Further investigating the Zernike coefficients that correspond to these aberrations, the strong spectral dependence of the amplitude of the aberration (see Fig. 6) is visible. This spectral

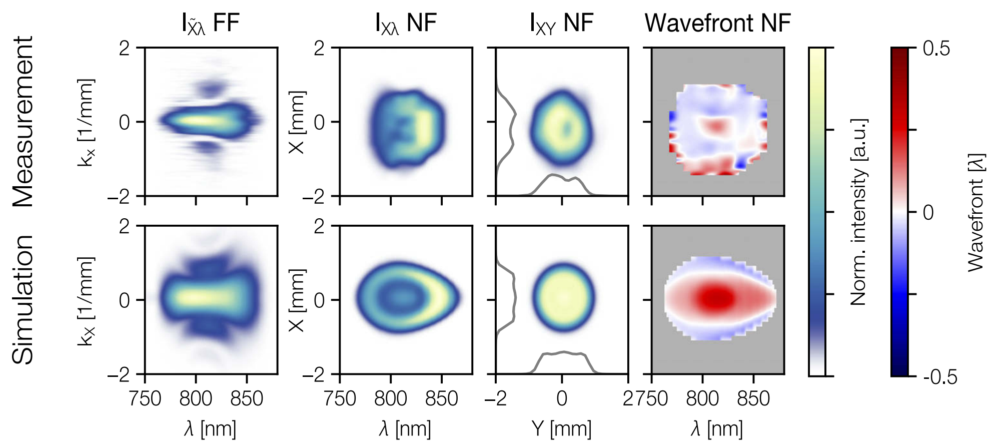

Fig. 5. Comparison of measured (top) and simulated (bottom) spectrally resolved beam profiles and wavefront. The top row shows the reconstructed spectrally resolved intensity profiles in the far-field (FF) and the near-field (NF), as well as the reconstructed beam profile of the NF beam imaged at the output surface of the OPA crystal. The last column shows the corresponding wavefront error in the near field as a function of wavelength (limited to region with intensity larger than 10% of peak intensity). The bottom row shows the corresponding profiles determined with the numerical simulations described in the previous section.

dependence leads to a degradation of the Strehl ratio across the spectrum, resulting in a Strehl-ratio of 0.85 at 803 nm, while the edges of the spectrum have a high wavefront quality with a Strehl-ratio of above 0.98.

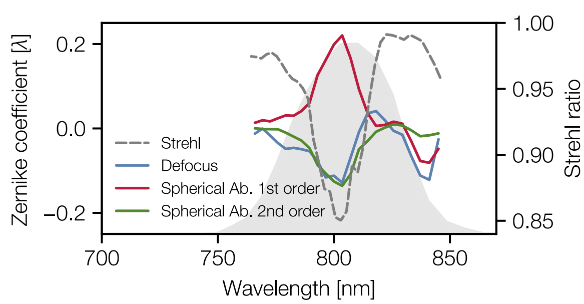

Fig. 6. Spectrally resolved magnitude of main aberrations, i.e. defocus and spherical aberration. The spectrally dependent aberrations result in a strong variation of the Strehl ratio across the spectrum.

5. Restoration of beam quality

To summarise the results so far, we can conclude that high energy stability of around 0.15 % is possible by strongly saturating an OPCPA amplifier. This however results in severe degradation of the beam quality, that manifests itself as a spectrally dependent deformation of the beam profile and wavefront of the output pulses.

When calculating the full spatio-spectral Strehl ratio S_{full}, as it was suggested by Giree *et al.* [28], one can see that the wavefront aberrations lead to a reduction in achievable peak intensity to 67 % compared to an aberration free pulse. In contrast to the spectrally averaged Strehl ratio $S_{\langle\omega\rangle}$, S_{full} is calculated by comparing the intensities achievable of the full spatio-spectral electric field of the distorted pulse, with that of the spectrally and spatially averaged field that corresponds to a pulse with a clean phase. This way, spectrally dependent phase aberrations such as chromatic aberration are considered in the calculation of the Strehl ratio, while they are omitted when spectrally averaging the single wavelength Strehl ratios to calculate $S_{\langle\omega\rangle}$. We calculate $S_{\langle\omega\rangle}$ by integrating

$$S_{\langle\omega\rangle} = \int I_{\mathrm{norm}}(\omega) e^{-\sigma_\phi(\omega)^2} d\omega, \tag{1}$$

where $I_{\mathrm{norm}}(\omega)$ is the normalized spectral intensity and $\sigma_\phi(\omega)$ denotes the standard deviation of the wavefront in a 4σ aperture of the beam [44] at the frequency ω.

$S_{\langle\omega\rangle}$ is calculated to be 0.92, indicating that the major influence on the degradation of the beam quality can be attributed to the chromaticity introduced by the saturation of the OPCPA process. This significant degradation of the achievable peak intensity, is a clear drawback of operating the OPCPA in saturation.

Spatial filtering of the beam after the final amplifier stage is a possible approach to improve the homogeneity of the beam properties across the spectrum and improve the overall beam quality. In particular filtering out the side-lobes visible in the far-field beam profile in Fig. 5 is expected to help. Additionally, such a scheme is easy to implement in the beam transport towards the next section of the amplification chain of the high energy laser system that is to be seeded. For the measurements shown in the following, a pinhole was placed in the Fourier plane of the transport towards the INSIGHT device that was described previously.

Already with a pinhole diameter of $D_{\mathrm{pinhole}} = 1.42\,w_0$ (1000 μm) and a high transmission through the filter of T = 92%, an immediate effect on the spectrally dependent Strehl ratio is visible (see Fig. 7). With a pinhole diameter of around $1.14\,w_0$ (800 μm), the Strehl ratio is above 0.98 across the entire spectrum, while the transmission is still at 85%. The full spatio-spectral Strehl in this filtered case is $S_{\mathrm{full}} = 0.85$, while the spectrally averaged Strehl is $S_{\langle\omega\rangle} = 0.99$. When comparing these values to those of the unamplified seed ($S_{\mathrm{full}} = 0.92$ and $S_{\langle\omega\rangle} = 0.94$), one can conclude that while the beam quality of individual spectral components is preserved or even slightly improved, there is some chromaticity introduced by the saturation that is not completely eliminated by the spatial filter.

As is shown in Fig. 7, the spectral variation of the spherical aberrations is however largely gone and an overall homogeneous spatio-spectral beam profile is achieved. This is visible in the FF and NF beam profiles, that both are close to a Gaussian profile across the entire spectrum, and the first and second order spherical aberrations maintain an amplitude below $\lambda/75$ and $\lambda/38$ respectively across the entire spectrum. In the unfiltered case the corresponding values were $\lambda/4.5$ and $\lambda/7$.

In addition to the improvement of the wavefront properties of the pulse, the shape of the spectrum is slightly changed as part of the energy in the distorted central part of the spectrum is not transmitted through the spatial filter. This leads to a flatting of the spectral shape (see Fig. 7), but does not have a significant influence on the spectral bandwidth.

Besides the improvement in beam quality, the spatial filtering could further reduce the 30 second energy jitter of the laser system by 20 % from 0.17 % rms to 0.14 % rms. These values are again close to the inherent noise and resolution limit of the diode based energy measurement and therefore provide an upper limit of the actual stability. This further improvement in energy stability is also observed in simulations and is attributed to the fact that once the back-conversion regime is reached, the input fluctuations primarily result in a fluctuation of the center of the beam profile, where the back-conversion occurs. Now propagating the beam to the Fourier plane, the small fluctuating central section of the pulse (that corresponds to higher spatial frequencies) is mapped to the side-lobes of the FF beam profile. By filtering these out, a significant fraction of the remaining energy fluctuations is eliminated.

Optics EXPRESS

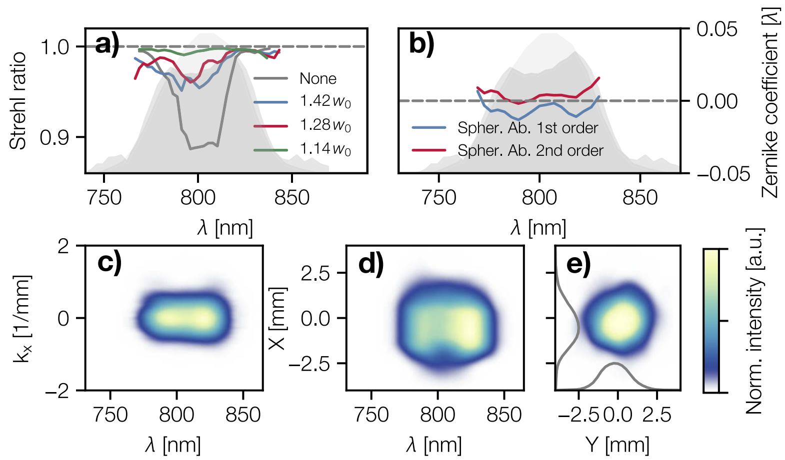

Fig. 7. Overview of the measured beam quality improvement after spatial filtering. Compared to Fig. 5, a great improvement in the homogeneity and the overall quality of the pulse is visible. a) shows the Strehl ratio across the spectrum for pinhole diameters from 1.14 w_0 to 1.42 w_0, as well as in the unfiltered case. w_0 is the 4σ beam diameter at the pinhole position. b) shows the residual wavefront error after filtering with the 1.14 w_0 pinhole and the bottom row shows the spectrally dependant beam profile in the far-field (c)) and the near-field beam (d)), as well as the NF beam profile (e) that corresponds to the collimated beam). The spectrum shown as an overlay in a) and b) is that of the beam filtered with the 1.14 w_0 pinhole, with the unfiltered spectrum shown in lighter grey in the background. The spectral wings visible around 750 nm and 850 nm in a) and b) are an artefact of the INSIGHT retrieval.

The trade-offs of the spatial filtering scheme entail on the one hand the above mentioned decrease in output energy (typically 10-20% depending on the exact configuration), and on the other hand an increased sensitivity of the laser performance on pointing fluctuations of the laser system. The improvement of short term jitter is thus only achievable, if the laser has a sufficient pointing stability. In the case of our specific laser system, the output pointing was measured to deviate well below 10 μrad over several hours.

Additionally, special care has to be taken to limit the in-focus intensity to prevent additional nonlinearities that could decrease the pulse quality. This concern can however easily be handled with the use of long focal lengths and potentially an in-vacuum spatial filter. Neither problems with pointing jitter of the laser, nor nonlinearities in the focal area were observed in our setup.

While this work focused on collinear OPAs, the investigated aberrations are also expected in non-collinear OPAs. Due to the additional walk-off between pump and seed pulses, the aberrations are then however not expected to be limited to the radially symmetric ones, but additionally aberrations such as coma should be present, in particular in the non-walkoff compensating phase matching scheme. Here, we concentrated on pulses with an spatial and temporal intensity close to a Gaussian profile. While this is typically the case for many OPA stages, a performance improvement is expected using spatio-temporally flat-top pump pulses, as they would lead to a more homogeneous saturation of the parametric amplification and therefore to a more homogeneous wavefront and beam profile. This would, however, demand dedicated measures for temporal and spatial beam shaping in the pump laser, that add complexity to the laser system.

Optics EXPRESS

6. Conclusion

In conclusion, we have presented a collinear OPCPA system dedicated to providing low-STC seed pulses with high energy stability to seed a high intensity laser amplification systems for laser-plasma acceleration. The laser system provides pulses centered at a wavelength of 800 nm that are compressible close to the Fourier limit of 24.8 fs and have a pulse energy of 46 μJ. A long-term shot-to-shot energy stability of 0.22 % was measured over 70 hours. To reach this high energy stability, the amplification process had to be saturated, which leads to aberrations of the intensity profile and wavefront of the pulse.

With the help of numerical simulations, we could show that these aberrations strongly vary across the spectrum of the pulse, which is attributed to the strongly varying intensity of the seed and pump pulses, as well as the phase matching curve that all contribute to spatially and spectrally varying amplification conditions of the laser pulses in the OPCPA. We further experimentally characterized these aberrations in the laser system with the help of the INSIGHT method. The resulting spectrally resolved beam profiles and wavefronts show good qualitative agreement with the features expected from the simulation. Finally, we showed that spatial filtering can be used to improve the spectral homogeneity and the the beam quality, such that a Strehl ratio of >0.98 is supported across the entire pulse spectrum. The Strehl ratio of the full spatio-spectral electric field after filtering, is measured to be 0.85. This spatial filtering also leads to a further improvement of the short term energy stability of the laser pulses to 0.14 % rms over 30 s.

Funding. Bundesministerium für Bildung und Forschung (05K19GUD).

Acknowledgments. We thank Spencer W. Jolly (ULB, Brussels), Ingmar Hartl (DESY, Hamburg) and Mikhail Pergament (DESY, Hamburg) for helpful discussions.

Disclosures. The authors declare no conflicts of interest.

Data availability. Data underlying the results presented in this paper are not publicly available at this time but may be obtained from the authors upon reasonable request.

References

1. T. Kobayashi, "Development of ultrashort pulse lasers for ultrafast spectroscopy," Photonics **5**(3), 19 (2018).
2. J. Lloyd-Hughes, P. M. Oppeneer, T. P. dos Santos, A. Schleife, S. Meng, M. A. Sentef, M. Ruggenthaler, A. Rubio, I. Radu, M. Murnane, X. Shi, H. Kapteyn, B. Stadtmüller, K. M. Dani, F. H. da Jornada, E. Prinz, M. Aeschlimann, R. L. Milot, M. Burdanova, J. Boland, T. Cocker, and F. Hegmann, "The 2021 ultrafast spectroscopic probes of condensed matter roadmap," J. Phys.: Condens. Matter **33**(35), 353001 (2021).
3. D.-S. Yang, O. F. Mohammed, and A. H. Zewail, "Scanning ultrafast electron microscopy," Proc. Natl. Acad. Sci. **107**(34), 14993–14998 (2010).
4. T. Tajima and J. M. Dawson, "Laser electron accelerator," Phys. Rev. Lett. **43**(4), 267–270 (1979).
5. E. Esarey, C. B. Schroeder, and W. P. Leemans, "Physics of laser-driven plasma-based electron accelerators," Rev. Mod. Phys. **81**(3), 1229–1285 (2009).
6. A. Popp, J. Vieira, J. Osterhoff, Z. Major, R. Hörlein, M. Fuchs, R. Weingartner, T. P. Rowlands-Rees, M. Marti, R. A. Fonseca, S. F. Martins, L. O. Silva, S. M. Hooker, F. Krausz, F. Grüner, and S. Karsch, "All-optical steering of laser-wakefield-accelerated electron beams," Phys. Rev. Lett. **105**(21), 215001 (2010).
7. M. Thévenet, D. E. Mittelberger, K. Nakamura, R. Lehe, C. B. Schroeder, J.-L. Vay, E. Esarey, and W. P. Leemans, "Pulse front tilt steering in laser plasma accelerators," Phys. Rev. Accel. Beams **22**(7), 071301 (2019).
8. C.-Q. Zhu, J.-G. Wang, Y.-F. Li, J. Feng, D.-Z. Li, Y.-H. He, J.-H. Tan, J.-L. Ma, X. Lu, Y.-T. Li, and L.-M. Chen, "Optical steering of electron beam in laser plasma accelerators," Opt. Express **28**(8), 11609–11617 (2020).
9. D. E. Mittelberger, M. Thévenet, K. Nakamura, A. J. Gonsalves, C. Benedetti, J. Daniels, S. Steinke, R. Lehe, J.-L. Vay, C. B. Schroeder, E. Esarey, and W. P. Leemans, "Laser and electron deflection from transverse asymmetries in laser-plasma accelerators," Phys. Rev. E **100**(6), 063208 (2019).
10. A. R. Maier, N. M. Delbos, T. Eichner, L. Hübner, S. Jalas, L. Jeppe, S. W. Jolly, M. Kirchen, V. Leroux, P. Messner, M. Schnepp, M. Trunk, P. A. Walker, C. Werle, and P. Winkler, "Decoding sources of energy variability in a laser-plasma accelerator," Phys. Rev. X **10**(3), 031039 (2020).
11. M. Kirchen, S. Jalas, P. Messner, P. Winkler, T. Eichner, L. Hübner, T. Hülsenbusch, L. Jeppe, T. Parikh, M. Schnepp, and A. R. Maier, "Optimal beam loading in a laser-plasma accelerator," Phys. Rev. Lett. **126**(17), 174801 (2021).
12. V. Leroux, T. Eichner, and A. R. Maier, "Description of spatio-temporal couplings from heat-induced compressor grating deformation," Opt. Express **28**(6), 8257–8265 (2020).

Optics EXPRESS

13. Z. Li, K. Tsubakimoto, H. Yoshida, Y. Nakata, and N. Miyanaga, "Degradation of femtosecond petawatt laser beams: Spatio-temporal/spectral coupling induced by wavefront errors of compression gratings," Appl. Phys. Express **10**(10), 102702 (2017).
14. A. Dubietis, G. Jonušauskas, and A. Piskarskas, "Powerful femtosecond pulse generation by chirped and stretched pulse parametric amplification in BBO crystal," Opt. Commun. **88**(4-6), 437–440 (1992).
15. I. Jovanovic, B. J. Comaskey, C. A. Ebbers, R. A. Bonner, D. M. Pennington, and E. C. Morse, "Optical parametric chirped-pulse amplifier as an alternative to Ti:sapphire regenerative amplifiers," Appl. Opt. **41**(15), 2923 (2002).
16. I. Ross, P. Matousek, M. Towrie, A. Langley, and J. Collier, "The prospects for ultrashort pulse duration and ultrahigh intensity using optical parametric chirped pulse amplifiers," Opt. Commun. **144**(1-3), 125–133 (1997).
17. J. Collier, C. Hernandez-Gomez, I. N. Ross, P. Matousek, C. N. Danson, and J. Walczak, "Evaluation of an ultrabroadband high-gain amplification technique for chirped pulse amplification facilities," Appl. Opt. **38**(36), 7486–7493 (1999).
18. C. Dorrer, I. A. Begishev, A. V. Okishev, and J. D. Zuegel, "High-contrast optical-parametric amplifier as a front end of high-power laser systems," Opt. Lett. **32**(15), 2143–2145 (2007).
19. C. Manzoni and G. Cerullo, "Design criteria for ultrafast optical parametric amplifiers," J. Opt. **18**(10), 103501 (2016).
20. D. Rivas, A. Borot, D. Cardenas, G. Marcus, X. Gu, D. Herrmann, J. Xu, J. Tan, D. Kormin, G. Ma, W. Dallari, G. Tsakiris, I. Földes, S.-W. Chou, M. Weidman, B. Bergues, T. Wittmann, H. Schröder, P. Tzallas, D. Charalambidis, O. Razskazovskaya, V. Pervak, F. Krausz, and L. Veisz, "Next generation driver for attosecond and laser-plasma physics," Sci. Rep. **7**(1), 5224 (2017).
21. A. Baltuška and T. Kobayashi, "Adaptive shaping of two-cycle visible pulses using a flexible mirror," Appl. Phys. B **75**(4-5), 427–443 (2002).
22. A. Shirakawa, I. Sakane, M. Takasaka, and T. Kobayashi, "Sub-5-fs visible pulse generation by pulse-front-matched noncollinear optical parametric amplification," Appl. Phys. Lett. **74**(16), 2268–2270 (1999).
23. A. Zaukevičius, V. Jukna, R. Antipenkov, V. Martinenaite, A. Varanavičius, A. P. Piskarskas, and G. Valiulis, "Manifestation of spatial chirp in femtosecond noncollinear optical parametric chirped-pulse amplifier," J. Opt. Soc. Am. B **28**(12), 2902 (2011).
24. O. Isaienko and E. Borguet, "Pulse-front matching of ultrabroadband near-infrared noncollinear optical parametric amplified pulses," J. Opt. Soc. Am. B **26**(5), 965–972 (2009).
25. J. Bromage, C. Dorrer, and J. D. Zuegel, "Angular-dispersion-induced spatiotemporal aberrations in noncollinear optical parametric amplifiers," Opt. Lett. **35**(13), 2251 (2010).
26. S. Zhang, M. Fujita, M. Yamanaka, M. Nakatsuka, Y. Izawa, and C. Yamanaka, "Study of the stability of optical parametric amplification," Opt. Commun. **184**(5-6), 451–455 (2000).
27. P. Fischer, A. Muschet, T. Lang, R. Salh, and L. Veisz, "Saturation control of an optical parametric chirped-pulse amplifier," Opt. Express **29**(3), 4210 (2021).
28. A. Giree, M. Mero, G. Arisholm, M. J. J. Vrakking, and F. J. Furch, "Numerical study of spatiotemporal distortions in noncollinear optical parametric chirped-pulse amplifiers," Opt. Express **25**(4), 3104 (2017).
29. Y. Wang, J. Wang, B. Zhou, J. Ma, P. Yuan, and L. Qian, "Spatiotemporal couplings through a nonlinear phase in broadband optical parametric amplification," Opt. Lett. **46**(22), 5743–5746 (2021).
30. N. Delbos, C. Werle, I. Dornmair, T. Eichner, L. Hübner, S. Jalas, S. Jolly, M. Kirchen, V. Leroux, P. Messner, M. Schnepp, M. Trunk, P. Walker, P. Winkler, and A. Maier, "Lux – a laser–plasma driven undulator beamline," Nucl. Instrum. Methods Phys. Res., Sect. A **909**, 318–322 (2018).
31. T. Hülsenbusch, Manuscript in preparation.
32. T. Lang, A. Harth, J. Matyschok, T. Binhammer, M. Schultze, and U. Morgner, "Impact of temporal, spatial and cascaded effects on the pulse formation in ultra-broadband parametric amplifiers," Opt. Express **21**(1), 949 (2013).
33. M. Guardalben, J. Keegan, L. Waxer, V. Bagnoud, I. Begishev, J. Puth, and J. Zuegel, "Design of a highly stable, high-conversion-efficiency, optical parametric chirped-pulse amplification system with good beam quality," Opt. Express **11**(20), 2511 (2003).
34. J. Moses, S.-W. Huang, K.-H. Hong, O. D. Mücke, E. L. F. ao Filho, A. Benedick, F. O. Ilday, A. Dergachev, J. A. Bolger, B. J. Eggleton, and F. X. Kärtner, "Highly stable ultrabroadband mid-IR optical parametric chirped-pulse amplifier optimized for superfluorescence suppression," Opt. Lett. **34**(11), 1639–1641 (2009).
35. F. Tavella, A. Marcinkevičius, and F. Krausz, "Investigation of the superfluorescence and signal amplification in an ultrabroadband multiterawatt optical parametric chirped pulse amplifier system," New J. Phys. **8**(10), 219 (2006).
36. J. Moses, C. Manzoni, S.-W. Huang, G. Cerullo, and F. X. Kaertner, "Temporal optimization of ultrabroadband high-energy OPCPA," Opt. Express **17**(7), 5540 (2009).
37. P. Hamm, R. A. Kaindl, and J. Stenger, "Noise suppression in femtosecond mid-infrared light sources," Opt. Lett. **25**(24), 1798 (2000).
38. R. Budriūnas, T. Stanislauskas, J. Adamonis, A. Aleknavičius, G. Veitas, D. Gadonas, S. Balickas, A. Michailovas, and A. Varanavičius, "53 W average power CEP-stabilized OPCPA system delivering 5.5 TW few cycle pulses at 1 kHz repetition rate," Opt. Express **25**(5), 5797–5806 (2017).
39. N. Thiré, R. Maksimenka, B. Kiss, C. Ferchaud, G. Gitzinger, T. Pinoteau, H. Jousselin, S. Jarosch, P. Bizouard, V. Di Pietro, E. Cormier, K. Osvay, and N. Forget, "Highly stable, 15 W, few-cycle, 65 mrad CEP-noise mid-IR OPCPA for statistical physics," Opt. Express **26**(21), 26907 (2018).

Optics EXPRESS

40. H. J. Bakker, P. C. M. Planken, L. Kuipers, and A. Lagendijk, "Phase modulation in second-order nonlinear-optical processes," Phys. Rev. A **42**(7), 4085–4101 (1990).
41. V. Leroux, https://github.com/VincentLeroux/Laser.
42. A. Borot and F. Quéré, "Spatio-spectral metrology at focus of ultrashort lasers: a phase-retrieval approach," Opt. Express **26**(20), 26444–26461 (2018).
43. A. Jeandet, A. Borot, K. Nakamura, S. W. Jolly, A. J. Gonsalves, C. Tóth, H.-S. Mao, W. P. Leemans, and F. Quéré, "Spatio-temporal structure of a petawatt femtosecond laser beam," JPhys Photonics **1**(3), 035001 (2019).
44. V. N. Mahajan, "Strehl ratio for primary aberrations in terms of their aberration variance," J. Opt. Soc. Am. **73**(6), 860–861 (1983).